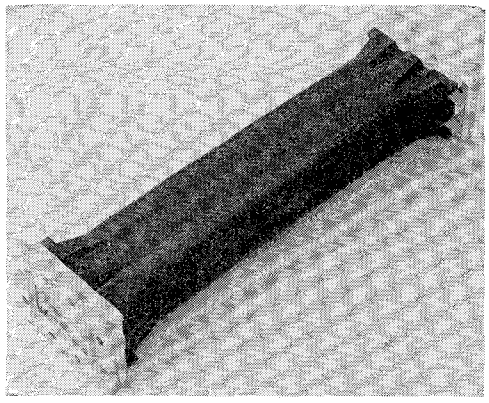

Fig. 17—Same double-ridge flexible waveguide with jacketing.

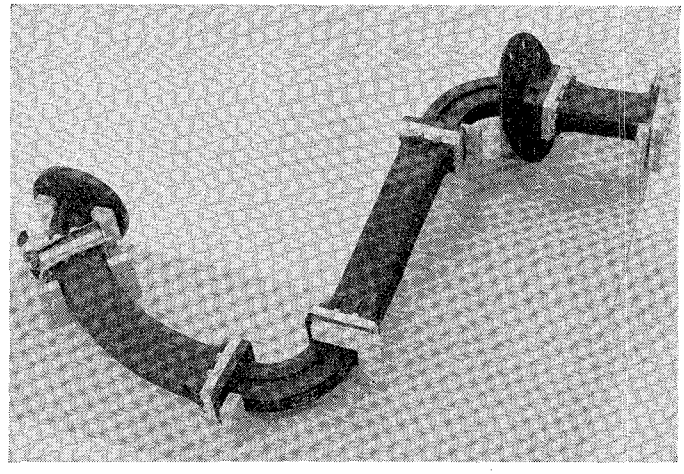

Fig. 18—Typical aircraft installation of double-ridge waveguide.

reflectometer and VSWR introducer near the TR unit so as to provide for matching the line—this to be checked at suitable intervals in a maintenance schedule. This would allow for discontinuities and irregularities that occur with usage in the aircraft. Another application might be to provide a pulse type high-level ferrite isolator so as to isolate the magnetron from the effect of discontinuities. This latter application has considerable promise although the complexities of an additional pulser and the weight of such a unit may make its use prohibitive.

Waveguide Miniaturization

One of the paramount advantages for double-ridge guide in this aircraft installation has been the size reduction possible without much sacrifice in peak power handling capabilities or attenuation for a practical radar application. A method is in sight for reducing the complexity of aircraft installation for lower frequency radar systems operating at 10 cm and perhaps even 30 cm. By use of similar techniques, extremely high peak power performance can be obtained from such structures at considerable saving in size and weight, and by using a two piece (Airtron type *S*) flexible guide construction, it should be possible to fabricate flexible guides and thus make installations in modern aircraft practical. The contributions of Mr. W. T. Carnes, Chairman of the Airlines Electronic Engineering Committee in co-ordinating and adapting this double-ridge guide are here gratefully acknowledged.

Bibliography

1. Cohn, S. B., "Properties of Ridge Waveguide." Proceedings of the IRE, Vol. 35 (August, 1947), pp. 783–788.
2. *Ridged Waveguide—A Transmission for a Wider Frequency Range.* PRD Reports, Vol. 1, No. 2 (July, 1952).
3. Ramo, S., and Whinney, J. R., *Fields and Waves in Modern Radio.* New York, John Wiley and Sons, Inc., 1953.
4. Marcuvitz, N., *Waveguide Handbook.* New York, McGraw-Hill Book Co., Inc., 1951.
5. *5.7 Cm Weather Penetration Airborne Radar.* ARINC Characteristic No. 529.

Simplified Calculation of Antenna Patterns, with Application to Radome Problems*

J. H. RICHMOND†

Summary—Generally, the calculation of antenna far-field patterns from known near-field distributions is tedious and may require the use of a large computer. The calculations are simplified for certain types of antennas having separable near fields. This simplifying assumption is found to yield satisfactory results with pyramidal horns and parabolic reflector antennas. Calculations are further simplified by approximating a complex line integral with two real summations.

Measured and calculated far-field patterns are included to indicate the accuracy of the calculations. Results are presented for horns and parabolic antennas and for a horn covered with a hollow dielectric wedge. The method is applicable to both *E*-plane and *H*-plane pattern calculations. The main lobe of a far-field pattern is calculated in less than one hour on a desk calculating machine by the simplified method. In radome work an important feature is that it permits rapid evaluation of the far-field distortion associated with any given near-field distortion in any given small region in the near field.

* The research reported in this paper was sponsored by the Air Res. and Dev. Command, Wright Air Dev. Center, Wright-Patterson AFB, Ohio.

† Antenna Lab., Dept. Elec. Engrg., Ohio State Univ., Columbus, Ohio.

Introduction

THE FOLLOWING problem frequently arises in antenna work. Given the tangential electric and magnetic field intensity distributions on some surface *S* enclosing an antenna, calculate the far-field pat-

tern of the antenna. While the solution may be simple in principle, in practice the numerical computation is tedious and may require the use of large computers. The problem is simplified if the surface S is chosen to be a plane. A knowledge of the tangential electric and magnetic fields on the plane is sufficient to determine the far field in the half-space not including the antenna.

Suppose that the tangential electric field is given over the yz-plane shown in Fig. 1. The E-plane and H-plane ($\phi=0$ and $\phi=90$-degree planes, respectively) relative far-field patterns associated with the z-polarized component $E_z(y, z)$ of the near field are given respectively by

$$E_\theta(\theta) = \int\int E_z(y, z)\epsilon^{j\beta z\cos\theta}dydz, \tag{1a}$$

and

$$E_\theta(\phi) = \int\int E_z(y, z)\epsilon^{j\beta y\sin\phi}dydz. \tag{1b}$$

Similar formulas give the E- and H-plane patterns $E_\phi(\theta)$ and $E_\phi(\phi)$ associated with a y-polarized near field. By superposition of the far fields associated with these two near-field components, the resultant far-field pattern is obtained even for elliptically polarized antennas. Hence, it will be sufficient to consider only linearly polarized fields.

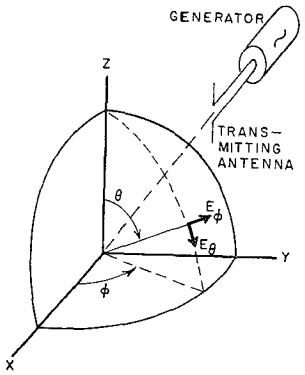

Fig. 1—Co-ordinates used in far-field calculations.

Now, unless $E_z(y, z)$ is a particularly simple function, the double integrations involved in (1) are laborious to evaluate. A simplification can be achieved, however, in certain practical cases where the near field is separable, that is,

$$E_z(y, z) = Y(y)Z(z). \tag{2}$$

In this event, (1a) and reduce to

$$E_\theta(\theta) = \int Z(z)\epsilon^{j\beta z\cos\theta}dz, \tag{3a}$$

and

$$E_\theta(\phi) = \int Y(y)\epsilon^{j\beta y\sin\phi}dy. \tag{3b}$$

The separability assumption has been found to yield satisfactory results in the case of pyramidal horns and small parabolic reflector antennas.

If the notation $Y(y)$ is replaced with $E_z(y)$, (3b) can be written

$$E_\theta(\phi) = \int E_z(y)\cos(\beta y\sin\phi)dy + j\int E_z(y)\sin(\beta y\sin\phi)dy. \tag{4}$$

A rapid approximate method of evaluating the first integral in (4) will next be described. The method can immediately be applied to the second integral in (4) and hence to the integrals in (3).

Simplified Approximate Far-Field Calculations

As shown, integrals of the following form appear in the far-field expressions:

$$E_\theta'(\phi) = \int E_z(y)\cos(\beta y\sin\phi)dy. \tag{5}$$

Many antennas set up near fields $E_z(y)$ which are symmetrical. In this case, (5) gives the H-plane far-field pattern. If α denotes the phase of $E_z(y)$, the near field can be resolved into real and imaginary components as follows.

$$E_z(y) = |E_z|(\cos\alpha + j\sin\alpha) = \Re[E_z] + j\Im[E_z]. \tag{6}$$

Thus, the complex integral (5) can be resolved into two real integrals and, for small values of y_0, can be approximated by the real summations:

$$E_\theta(\phi) \approx \sum_{k=1,3,5,\cdots}^{n} \{\Re[E_z(ky_0)] + j\Im[E_z(ky_0)]\}\cos(\beta ky_0\sin\phi). \tag{7}$$

Any desired degree of approximation can be obtained by choosing y_0 small enough; however, the labor involved increases as y_0 is decreased.

If the value chosen for y_0 is greater than about 0.1 wavelength, a better approximation to (5) is given by

$$E_\theta(\phi) = \sum_{k=1,3,5,\cdots}^{n} \{\bar{\Re}[E_z(ky_0)] + j\bar{\Im}[E_z(ky_0)]\}A_k(\phi) \tag{8}$$

where $\bar{\Re}[E_z(ky_0)]$ and $\bar{\Im}[E_z(ky_0)]$ denote the average values of the real and imaginary components, respectively, over the interval $(k-1)y_0<y<(k+1)y_0$, and

$$A_k(\phi) = \int_{(k-1)y_0}^{(k+1)y_0} \cos(\beta y\sin\phi)dy. \tag{9}$$

If (8) is used, the continuous near-field distribution $E_z(y)$ is in effect approximated by an array of uniformly-excited line sources, each of length $2y_0$ and of the proper strength. The relative far-field patterns of these line sources are precisely the $A_k(\phi)$, and (8)

superimposes the individual far-field contributions in their proper strengths. The summation must be extended along the y-axis to a point where $|E_z|$ becomes and remains negligible. Satisfactory results have been obtained by carrying the summation out to a point where $|E_z|$ becomes and remains less than 1 per cent of its maximum value.

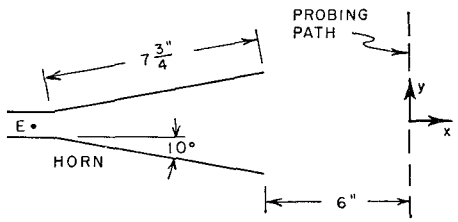

Fig. 2—Pyramidal horn antenna used to test the far-field calculation method.

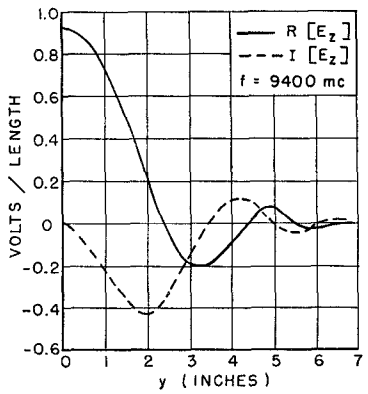

Fig. 3—Measured near fields of horn antenna shown in Fig. 2.

The far-field calculation method was tested at X-band on the horn antenna shown in Fig. 2. The near field $E_z(y)$ was measured with a small open-ended waveguide probe[1] along a path 6 inches from the horn aperture. For convenience in performing the calculations, the real and imaginary components of E_z were measured directly rather than the amplitude and phase. This was done by using a phase-sensitive coherent detector[2] which actually requires less elaborate equipment than that of a linear receiver or a phase plotter. These measured near fields are reproduced in Fig. 3. Using the measured near fields, the H-plane far-field pattern of the horn was calculated from (7) with $y_0 = 0.1$ inch and from (8) with $y_0 = 0.25$ inch and 0.5 inch. The measured pattern and the three calculated patterns are compared in Fig. 4. The measurements and calculations were carried out only through the main lobe of the far-field pattern since only this region was of interest in the work at hand.

[1] J. H. Richmond and T. E. Tice, "Probes for microwave near-field measurements," *Trans. IRE*, vol. MTT-3, pp. 32–34; April, 1955.

[2] J. H. Richmond, "Measurement of time-quadrature components of microwave signals," *Trans. IRE*, vol. MTT-3, pp. 13–15; April, 1955.

Of course, the largest value of y_0 which will give accurate far-field calculations depends on the nature of the particular near-fields involved. It may be practical to use a larger value of y_0 when working with fields which vary more slowly with y. In the example shown in Fig. 4, when y_0 is reduced to 0.1 inch (about 0.08λ) the error arising from replacement of the integral in (5) with the summation in (7) diminishes to the same order of magnitude as the experimental errors involved in measuring the near and far fields.

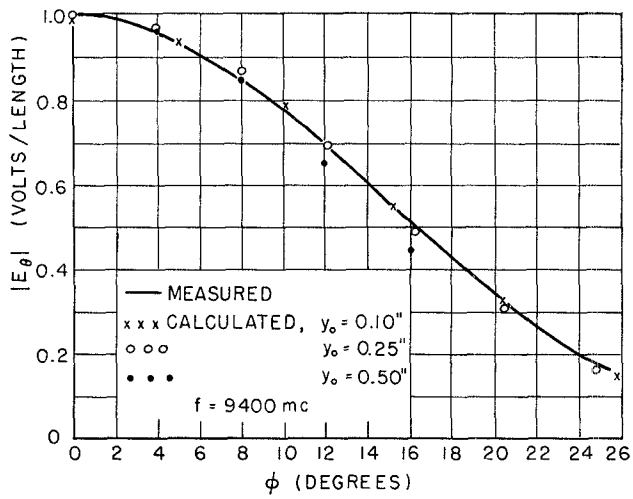

Fig. 4—Measured and calculated H-plane far-field patterns of horn shown in Fig. 2.

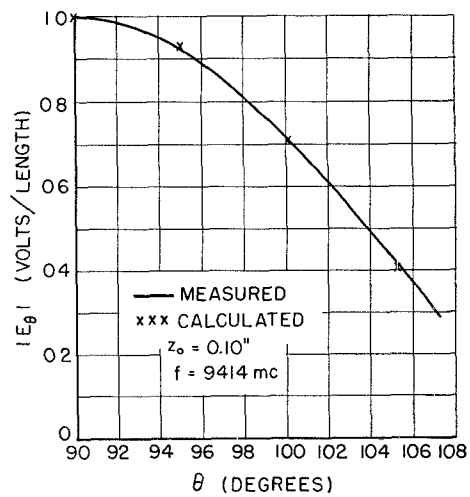

Fig. 5—E-plane far-field pattern of horn antenna shown in Fig. 2.

Examples

To indicate the usefulness and accuracy of the simplified calculations, several examples are presented. Fig. 5 shows the measured and calculated E-plane far-field patterns of the horn antenna of Fig. 2. The calculations were based on the near fields $E_z(z)$ measured on a line 6 inches from the horn aperture. A formula similar to (7) was derived from (3a) and was used for the E-plane calculations.

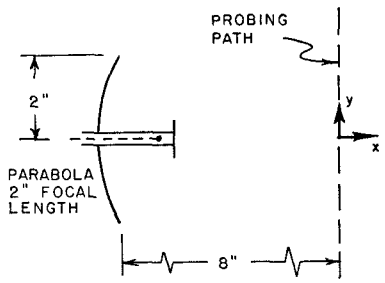

Fig. 6—Parabolic antenna used to test the far-field calculations.

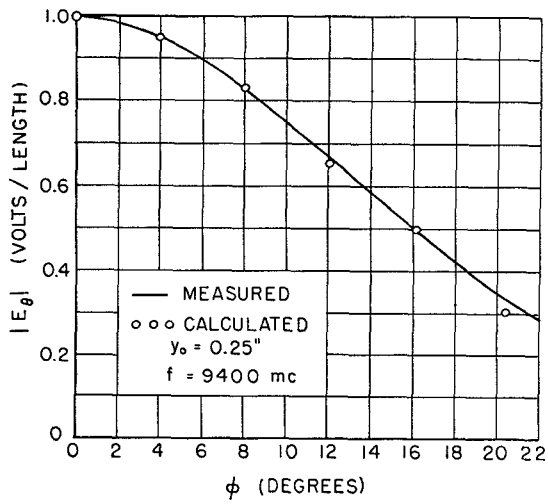

Fig. 7—*H*-plane far-field pattern of parabolic antenna shown in Fig. 6.

Eq. (8) was used to calculate the *H*-plane far-field pattern of the small parabolic antenna which is shown in Fig. 6. The measured and calculated patterns are shown in Fig. 7.

Finally, a hollow dielectric wedge was placed over a horn antenna as shown in Fig. 8. The measured and calculated far fields (8) are shown in Fig. 9. The far-field pattern of the horn alone is also shown for comparison. In the case of the horn with the dielectric wedge, the calculations do not agree with measured far fields quite as perfectly as in the other examples. Although the discrepancy is small, it should be stated that it is not entirely attributable to the approximations which are made in the calculations. Some portion of the error undoubtedly arises from imperfect near- and far-field measurements.

Conclusions

A rapid approximate method of calculating the far-field patterns of certain types of antennas is developed. The near fields are assumed to be known, and simplification is achieved by the following procedure:

1. Choose a plane as the surface on which the near fields are to be given;
2. Assume that the near fields are separable;
3. Approximate the far-field integral with a summation, and use the least possible number of terms consistent with the accuracy desired;
4. Resolve the complex summation into two real summations, thus minimizing the amount of vector addition involved; and
5. Measure the real and imaginary components of the near field directly with a phase-sensitive detector, rather than computing these functions from measured phase and amplitude patterns.

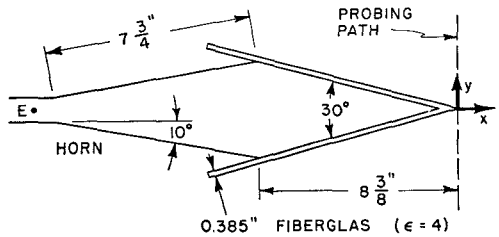

Fig. 8—Horn antenna and hollow dielectric wedge used to test the far-field calculations.

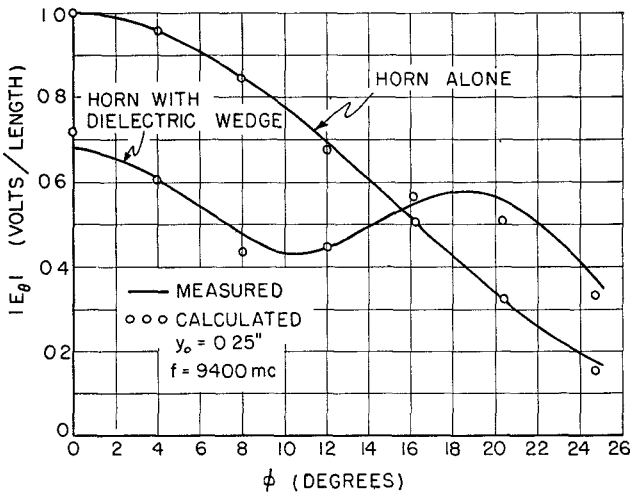

Fig. 9—*H*-plane far-field patterns of horn with and without dielectric wedge.

As a result, far-field patterns can be calculated through the main lobe in less than one hour on a desk calculating machine. Both *E*-plane and *H*-plane calculations have been carried out successfully. The calculations agree satisfactorily with measured far-field patterns for horns and parabolic reflector antennas, for example, as well as for a horn covered with a hollow dielectric wedge. In radome work an important feature of the method is that it permits rapid evaluation of the far-field distortion associated with any given near-field distortion in any given small region in the near field.